RAA 2019 Vol. **19** No. **10**, 141(8pp) doi: 10.1088/1674–4527/19/10/141

http://www.raa-journal.org *http://iopscience.iop.org/raa*

***R**esearch in*
***A**stronomy and*
***A**strophysics*

Unusual infrared emission toward Sgr B2: possible planar C_{24}

Xiu-Hui Chen[1,2], Fu-Yuan Xiang[1], Xue-Juan Yang[1] and Aigen Li[2]

[1] Department of Physics, Xiangtan University, Xiangtan 411105, China; *chenxh@smail.xtu.edu.cn, fyxiang@xtu.edu.cn, xjyang@xtu.edu.cn*

[2] Department of Physics and Astronomy, University of Missouri, Columbia, MO 65211, USA; *lia@missouri.edu*

Received 2019 February 22; accepted 2019 May 5

Abstract Interstellar graphene could be present in the interstellar medium (ISM), resulting from the photochemical processing of polycyclic aromatic hydrocarbon (PAH) molecules and/or collisional fragmentation of graphitic particles. Indeed, by comparing the observed ultraviolet (UV) extinction and infrared (IR) emission of the diffuse ISM with that predicted for graphene, as much as $\sim 2\%$ of total interstellar carbon could be locked up in graphene without violating the observational constraints. While the possible detection of planar C_{24}, a small piece of a graphene sheet, has been reported towards several Galactic and extragalactic *planetary nebulae*, graphene has not yet been detected in *interstellar* environments. In this work, we search for the characteristic IR features of C_{24} at ~ 6.6, 9.8 and 20 μm toward Sgr B2, a high-mass star formation region, and find a candidate target toward R.A. (J2000) $= 267.05855^\circ$ and Decl. (J2000) $= -28.01479^\circ$ in Sgr B2 whose *Spitzer*/IRS spectra exhibit three bands peaking at ~ 6.637, 9.853 and 20.050 μm which appear to be coincident with those of C_{24}. Possible features of C_{60} are also seen in this region. The candidate region is a warm dust environment heated by massive stars or star clusters, associated with a *WISE* spot (a tracer of star formation activity), close to the HII region candidate IRAS 17450–2759, and is surrounded by seven young stellar object candidates within $\sim 5'$, suggesting that the creation and/or excitation of C_{24} could be related to star formation activities.

Key words: line: identification — ISM: lines and bands — ISM: molecules

1 INTRODUCTION

Carbon, with many allotropes known to be present in the interstellar medium (ISM; e.g., see Jäger et al. 2011), plays an important role in the physical and chemical evolution of the ISM (Henning & Salama 1998). Several carbon nanostructures such as polycyclic aromatic hydrocarbons (PAHs, e.g., Tielens 2008), nanodiamonds (Guillois et al. 1999; Van Kerckhoven et al. 2002), fullerenes (e.g., Cami et al. 2010; Sellgren et al. 2010; García-Hernández et al. 2010, 2011a; Zhang & Kwok 2011, 2013; Berné et al. 2017) and their ions (Foing & Ehrenfreund 1994; Berné et al. 2013; Campbell et al. 2015, 2016; Strelnikov et al. 2015) are promising carriers of many infrared (IR) emission features seen in the interstellar and circumstellar medium, although their exact identification still remains debated (e.g., Kwok & Zhang 2011; Yang et al. 2013; Rosenberg et al. 2014; Álvaro Galué & Díaz Leines 2017).

Graphene was first synthesized in the laboratory in 2004 by A.K. Geim and K.S. Novoselov (see Novoselov et al. 2004) for which they received the 2010 Nobel Prize in physics. García-Hernández et al. (2011b, 2012) first detected the unusual IR emission features at ~ 6.6, 9.8 and 20 μm in several Galactic and extragalactic planetary nebulae (PNe), which are coincident with the strongest transitions of a planar graphene sheet C_{24} theoretically predicted by Kuzmin & Duley (2011)[1]. More recently, Chen et al. (2017) studied the ultraviolet (UV) absorption and IR emission of graphene C_{24}. They estimated the abundance of graphene in the ISM to be < 5 ppm of C/H (i.e., $\sim 1.9\%$ of the total interstellar C) by comparing the observed UV

[1] A small planar graphene sheet is essentially a fully dehydrogenated PAH molecule. The planar C_{24} graphene can be considered as coronene whose hydrogen atoms are completely lost, differing from the small fullerene C_{24}. Bernstein et al. (2017) argued that the 11.3 μm feature, commonly attributed to PAHs, could also arise from fullerene C_{24}.

extinction and IR emission of the diffuse ISM with that predicted for graphene.

In principle, graphene could be present in the ISM as it could be formed from the photochemical processing of PAHs, which are abundant in the ISM, through a complete loss of their H atoms (e.g., Berné & Tielens 2012). Chuvilin et al. (2010) showed experimentally that C_{60} could be formed from a graphene sheet. Berné & Tielens (2012) further proposed that such a formation route could occur in space[2]. In these scenarios, the formation of C_{60} from graphene and the formation of graphene from PAHs are more likely to occur in regions rich in energetic UV photons. One such region is Sgr B2, a UV-rich high-mass star formation region. To this end, we search for the IR emission features of C_{24} towards Sgr B2.

Star formation activity is overall deficient in the Central Molecular Zone (CMZ) of the Galaxy relative to its gas abundance (Guesten & Downes 1983; Morris & Serabyn 1996; Kauffmann et al. 2017), challenging the empirical relationships between star formation rate and gas surface (Ginsburg et al. 2018). The distinctive physical and chemical parameters, such as pressure, temperature, velocity dispersion, abundances of elements, heating/cooling and chemical evolution, in the CMZ (Requena-Torres et al. 2006; Shetty et al. 2012; Grieco et al. 2015; Ginsburg et al. 2016; Henshaw et al. 2016; Tanaka et al. 2018, and references therein) are therefore of much interest. Most of the dust ridge clouds in the CMZ contain several thousand $M_{\odot}$ in stars or $< 8\%$ star-formation efficiency (Barnes et al. 2017). Despite the active star formation in Sgr B2 (which contains actively forming star clusters, high-mass young stellar objects (YSOs) and many compact HII regions, e.g., Gaume et al. 1995; Higuchi et al. 2015), the overall cloud appears to be as inefficient as the other dust ridge clouds. We are thus eager to investigate the environment in Sgr B2.

This paper is organized as follows. A brief description of spectroscopic data from the *Spitzer Space Telescope* (*Spitzer*) (Houck et al. 2004) that we used is presented in Section 2, while the associated search results are reported and discussed in Section 3. The main conclusion is given in Section 4.

[2] If a population of hydrogenated amorphous carbon (HAC)-like nanoparticles exists in the ISM with a mixed aromatic/aliphatic structure (e.g., Kwok & Zhang 2011), a complete loss of their H atoms could also convert HAC-like nanoparticles into graphene (e.g., García-Hernández et al. 2010, 2011b,a). Also, graphene could be generated in the ISM from the exfoliation of graphite as a result of grain-grain collisional fragmentation. It is worth noting that graphite is thought to be a major dust component in the ISM (Draine & Lee 1984) and, as mentioned earlier, presolar graphite grains have been identified in primitive meteorites.

2 DATA DESCRIPTION

The data analyzed here were obtained with the Infrared Spectrograph (IRS) on board *Spitzer* and are publicly available[3] (Houck et al. 2004; Werner et al. 2004). Data products from the short-low (SL) and long-low (LL) modules from the Spitzer Science Center (SSC) pipeline (version 18.18) were used to produce the final merged spectra, making use of the four slits: SL2 (5.21 – 7.56 μm) and SL1 (7.57 – 14.28 μm) with resolution $R \sim 100$, and LL2 (14.29 – 20.66 μm) and LL1 (20.67 – 38.00 μm) with resolution $R \sim 100$ (e.g., Simpson et al. 2007; Simpson 2018). In particular, the SL2, SL1 and LL2 slits cover wavelength regions with the most pronounced theoretical IR emission features of graphene C_{24} (i.e., at $\sim$6.6, 9.8 and 20 μm, see e.g., Martin et al. 1996; Kuzmin & Duley 2011; Chen et al. 2017 and references therein). We downloaded all the SL and LL data (103 pointings[4]) toward Sgr B2 and used the software MATLAB to extract spectral information from the original data.

We searched for the simultaneous presence of all three emission features of graphene C_{24} at $\sim$6.6, 9.8 and 20 μm and found only four Sgr B2 pointings which exhibit all these features (see Table 1)[5]. Table 1 lists the coordinates, minimum signal-to-noise ratio (S/N) of the four slits reported from the original downloaded data and the noise level at 1σ. Because the maximum distance between the four points is $\sim 0.7''$, we took the mean spectrum toward the four pointings and the central coordinate of the new target is R.A. (J2000) $= 267.05855°$ and Decl. (J2000) $= -28.01479°$. Figure 1 displays a three-color map featuring the target, where the blue, green and red images are from the 21 μm emission observed by the *Midcourse Space Experiment* (*MSX*; Price et al. 2001) and the 70 and 500 μm emission from the *Herschel Space Observatory* (Molinari et al. 2011).

3 RESULTS AND DISCUSSION

3.1 The Spectra

We detected three IR emission features near the most pronounced theoretical IR emission features of planar C_{24}

[3] Download from `http://sha.ipac.caltech.edu/applications/Spitzer/SHA/`.

[4] We have searched for the IRS Enhanced data towards Sgr B2 within a radius of $\sim 1°$ and obtained 103 pointings in total.

[5] The Principal Investigator (PI) for these *Spitzer*/IRS observations was Lee Armus with the Program ID 1405, 1412, 1413 and 1419 in stare mode. All the four pointings are towards the object HDE216285 entitled by the PI.

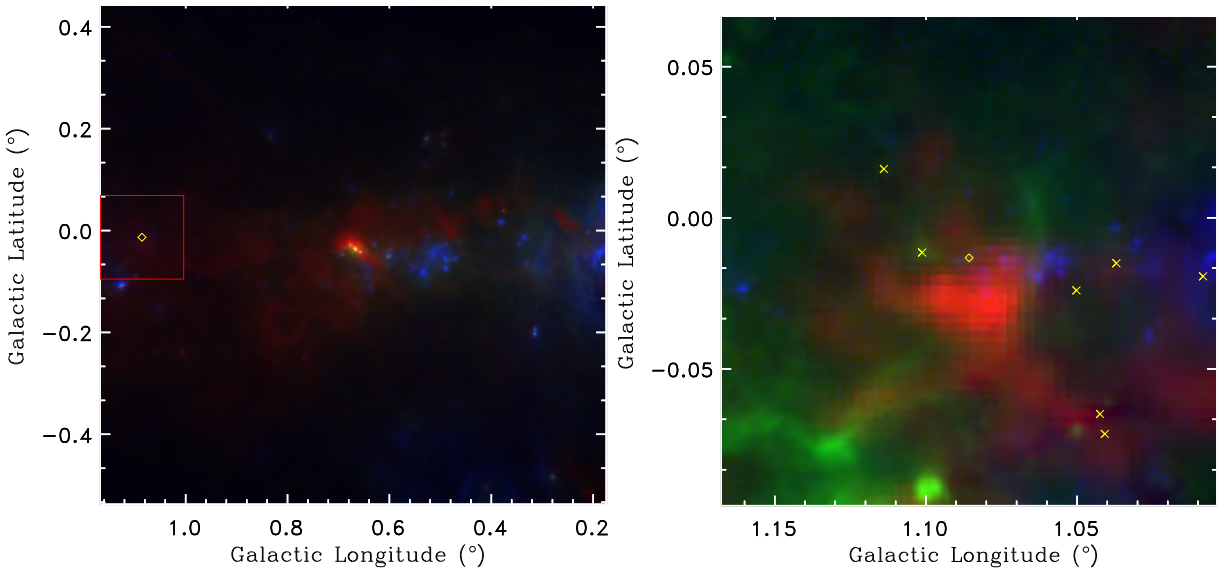

Fig. 1 Three-color images of the Sgr B2 region, where *blue* is the 21 μm Band-E MSX image (Price et al. 2001), *green* is the 70 μm image from the Herschel InfraRed Galactic Plane Survey (Hi-GAL Molinari et al. 2011) which is taken with the Photodetector Array Camera and Spectrometer (Poglitsch et al. 2010) on the *Herschel Space Observatory* (Pilbratt et al. 2010), and *red* is the 500 μm image from Hi-GAL acquired with the Spectral and Photometric Imaging Receiver (Griffin et al. 2010). The right panel is a close-up image of the *red box* in the left panel. The *diamond* marks the target, and the *crosses* signify possible YSOs (Robitaille et al. 2008; Yusef-Zadeh et al. 2009).

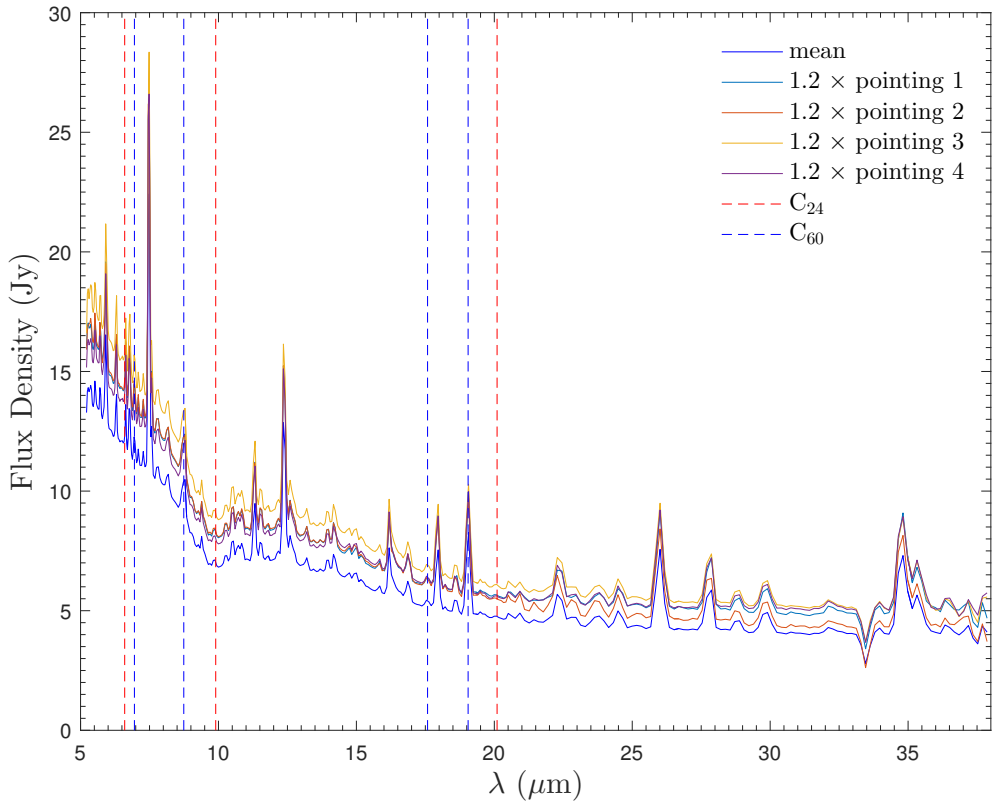

Fig. 2 The spectra of the four pointings with their flux density multiplied by 1.2 and the mean spectrum of the four pointings. The *red* and *blue dashed lines* indicate the possible C_{24} and C_{60} features, respectively.

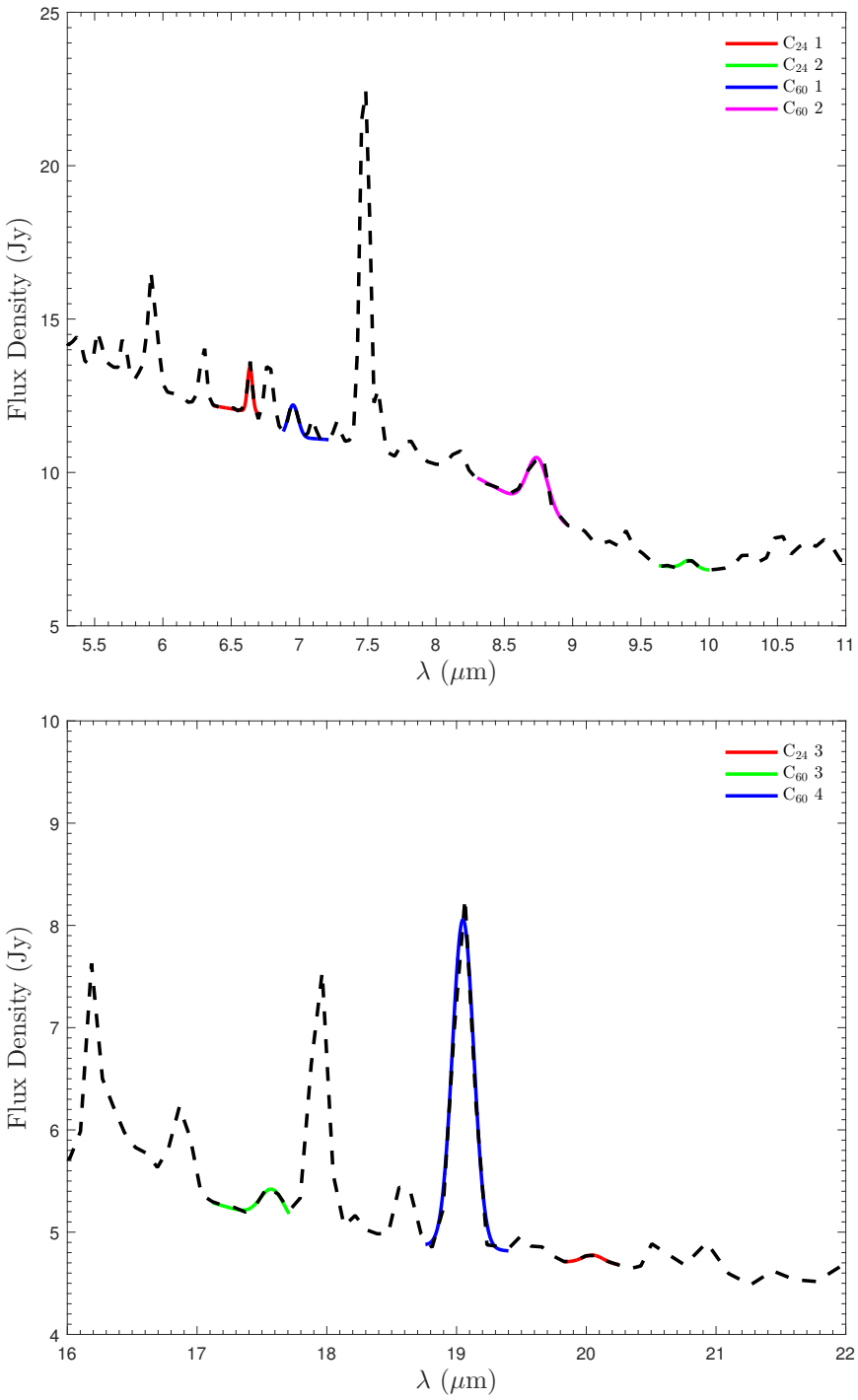

Fig. 3 The mean spectrum of the four pointings. The *color spectra* show the results of Gaussian fits for three components of C_{24} and four components of C_{60}.

Table 1 Information for Targets in Sgr B2

Index	R.A. (J2000) (degree)	Decl. (J2000) (degree)	S/N	σ (Jy)
1	267.05851	−28.01484	53	0.013
2	267.05847	−28.01476	53	0.013
3	267.05857	−28.01479	53	0.014
4	267.05866	−28.01478	53	0.013

(i.e., at ∼6.6, 9.8 and 20 μm, see e.g., Martin et al. 1996; Kuzmin & Duley 2011; Chen et al. 2017 and references therein) towards all the four pointings (see Fig. 2). In the following, we shall present the three components based on the mean spectrum in detail.

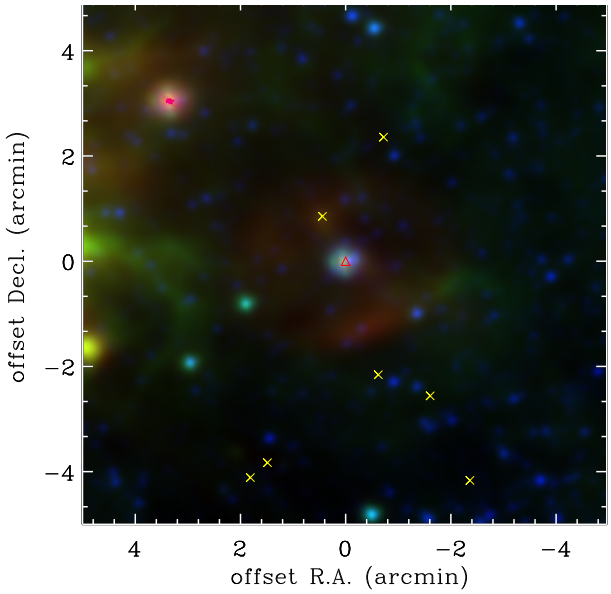

Fig. 4 Background false-color map centered on the target (*red triangle*) at R.A. (J2000) = 267.05855° and Decl. (J2000) = −28.01479°) with seven YSO candidates superimposed (*yellow crosses*, Robitaille et al. 2008; Yusef-Zadeh et al. 2009), where *blue* is the *WISE* 4.6 μm, *green* is the 12 μm and *red* is the 22 μm data.

We fit the spectra in terms of Gaussian profile (see Eq. (1)) in three windows centered at ∼6.64, 9.85 and 20.05 μm for C_{24}, where a linear baseline is used in these windows with small wavelength span (i.e., $\lesssim 1$ μm)

$$F_\lambda = A_0 \cdot \exp\left[-\left(\frac{\lambda-\lambda_0}{\Delta\lambda}\right)^2\right] + C_1 \cdot \lambda + C_2, \quad (1)$$

where A_0, C_1 and C_2 are constants, and λ_0 and $\Delta\lambda$ are respectively the peak wavelength and the width of the Gaussian profile. We find possible C_{24} emission toward Sgr B2 where the specified coordinates are described in Section 2. The mean spectrum of this candidate is shown in Figure 3 in detail. The results of the three components are cataloged in Table 2. Both A_0 for the three components are higher than 5σ. The three central wavelengths are all close to those with the most pronounced theoretical IR emission features of planar C_{24} (i.e., at ∼6.6, 9.8 and 20 μm, see e.g., Martin et al. 1996; Kuzmin & Duley 2011; Chen et al. 2017 and references therein). This suggests that those three components are likely to originate from planar C_{24}. The differences in the central wavelengths between the results reported in Table 2 and the theoretical central wavelengths may be due to the well-known fact that density functional theory (DFT) computation of C_{24} may not be precise in terms of wavelength (Borowski 2012).

The integrated intensity (I) ratios for C_{24} calculated from the fitted line are $I_1/I_2 \approx 2.2$ and $I_1/I_3 \approx 4.0$, where subscripts denote component indexes. The observed I_1/I_2 here is comparable to the theoretical value of ∼1.8, but the observed I_1/I_3 is higher than the theoretical value of ∼0.4 predicted for C_{24} excited by the interstellar radiation field of the general diffuse ISM (Chen et al. 2017). The band ratios are sensitive to the starlight spectral shape (i.e., "hardness") and, to a lesser degree, to the starlight intensity (see Draine & Li 2001). An exact match would require detailed IR emission modeling of C_{24} in Sgr B2 in the future.

Because C_{24} features have been detected in conjunction with fullerene features in Galactic and extragalactic PNe (García-Hernández et al. 2011b, 2012), we also fit the spectrum by Gaussian profiles (see Eq. (1)) in four windows centered at ∼7.0, 8.8, 17.4 and 18.9 μm for C_{60} (see Fig. 3). The results are cataloged in Table 3. The C_{60} integrated intensity ratios are $I_1/I_4 \sim 0.16$, $I_2/I_4 \sim 0.52$ and $I_3/I_4 \sim 0.11$. These band ratios differ from those of PNe (Sellgren et al. 2010) and reflection nebulae (Bernard-Salas et al. 2012). However, this could be simply due to the fact that the excitation condition of C_{60} varies between our target and those of PNe and reflection nebulae (Iglesias-Groth et al. 2011). Both the intensity and "hardness" of the starlight radiation fields to which C_{60} is exposed would affect the temperature distribution of C_{60}. Note that C_{60}, like C_{24} graphene, undergoes single-photon heating and the maximum temperature it attains is sensitive to the spectral shape of the illuminating starlight (see Draine & Li 2001).

The coexistence of C_{24} and C_{60} further confirms that the IR emission at ∼6.637, 9.853 and 20.050 μm may orig-

Table 2 Gaussian Fits to Three Possible Components of C_{24}

Components	λ_0 (μm)	$\Delta\lambda$ (μm)	A_0 (Jy)	C_1 (Jy μm^{-1})	C_2 (Jy)
1	6.637 ± 0.001	0.026 ± 0.001	1.463 ± 0.025	-0.747 ± 0.083	16.930 ± 0.540
2	9.853 ± 0.001	0.067 ± 0.002	0.260 ± 0.005	-0.383 ± 0.022	10.650 ± 0.210
3	20.050 ± 0.000	0.116 ± 0.002	0.082 ± 0.001	-0.711 ± 0.003	6.119 ± 0.066

Table 3 Gaussian Fits to Four Possible Components of C_{60}

Components	λ_0 (μm)	$\Delta\lambda$ (μm)	A_0 (Jy)	C_1 (Jy μm^{-1})	C_2 (Jy)
1	6.953 ± 0.001	0.053 ± 0.001	1.047 ± 0.022	-0.321 ± 0.102	13.380 ± 0.730
2	8.742 ± 0.001	0.107 ± 0.002	1.696 ± 0.024	-2.364 ± 0.056	29.450 ± 0.480
3	17.580 ± 0.000	0.130 ± 0.003	0.304 ± 0.008	-0.373 ± 0.023	11.680 ± 0.390
4	19.050 ± 0.000	0.115 ± 0.001	3.029 ± 0.011	-0.090 ± 0.019	6.564 ± 0.354

inate from planar C_{24}. García-Hernández et al. (2011b) propose that shocks which are driven by strong stellar winds can trigger processing of HACs. Fullerenes, possibly planar C_{24} molecules, and other complex aromatic and aliphatic species, could evolve from the vaporization of HACs.

As discussed above, we refer to the candidate carrier of the three components (centered at $\sim$6.637, 9.853 and 20.050 μm) as planar C_{24}. Further observations, especially with higher spectral resolution, and further experimental research and theoretical computation are required to confirm this.

3.2 Relation with Star-Formation Activity

The excitation of C_{24} requires UV photons. As illustrated in Figure 2 of Chen et al. (2017), C_{24} mostly absorbs in the far-UV. Therefore, in regions with intense star-formation activity, the excitation of C_{24} is naturally expected to occur. Also, the creation of C_{24} from PAHs, HAC and/or graphite is also more likely to occur in UV-rich regions.

In addition to the 21 μm, 70 and 500 μm images (see Fig. 1, Price et al. 2001; Molinari et al. 2011), we also provide high-sensitivity mid-IR images from the *Wide-field Infrared Survey Explorer* (*WISE*, see Fig. 4, Wright et al. 2010) to indicate the protostar activity. The candidate YSOs are superposed in these two figures. The 21 and 70 μm emissions show the warm dust heated by nearby massive stars or star clusters; and the far-IR emission (e.g. at 500 μm) that is from the cold dust signifies the locations of dense molecular clouds that have few indicators of active star formation (Simpson 2018 and references therein). As stated in Wright et al. (2010), the excesses at 12 μm and 22 μm bands are indicators of star formation activity. Both Figures 1 and 4 indicate that the target is probably impacted by star formation. The former delineates a star-forming region where the warm dust is heated by nearby massive stars or star clusters and is surrounded by cold dust. The excesses in the 12 μm and 22 μm bands in the latter also imply that the source is probably impacted by star formation.

The target region where C_{24} is seen is more likely associated with HII regions than PNe. The IRAS source (with an angular resolution of $\sim 0.75'$ – $3.0'$), IRAS 17450-2759, $13.7''$ away from the target manifests $F_{12}/F_{25} = 0.64$, $F_{25}/F_{60} = 0.06$, $F_{60}/F_{12} = 27.58$, $F_{100}/F_{12} = 112.74$, $F_{100}/F_{25} = 71.94$ and $F_{100}/F_{60} = 4.09$, where F_{12}, F_{25}, F_{60} and F_{100} denote the flux densities at 12, 25, 60 and 100 μm, respectively. The corresponding flux qualities are $Q_{12} = 3$, $Q_{25} = 2$, $Q_{60} = 1$ and $Q_{100} = 3$[6], respectively. Both of them conform with criteria of HII regions which are excited by embedded high mass stars (except $Q_{60} > 1$ is required in some criteria, see Yan et al. 2018) rather than properties of PNe (Kohoutek 2001).

We have also searched for YSOs from Simbad[7] within $5'$ of the target in this work. Seven YSO candidates[8] (Robitaille et al. 2008; Yusef-Zadeh et al. 2009) are surrounding the target, indicating that the candidate planar C_{24} emission is likely to be associated with star formation activity.

In addition, the 4.6, 12 and 22 μm filters from the *WISE* data include continuum emission from ultrasmall grains which undergo stochastic heating (Wright et al.

[6] The flux quality values of 1, 2 and 3 represent an upper limit, moderate quality and high quality, respectively (see `https://heasarc.gsfc.nasa.gov/W3Browse/all/iraspsc.html`).

[7] `http://simbad.u-strasbg.fr/simbad/sim-fcoo`

[8] SSTGC 891214, SSTGC 899543, SSTGC 909173, 2MASS J17480460–2805032, 2MASS J17480762–2803267 and 2MASS J17481157–2803027 from Yusef-Zadeh et al. (2009), and SSTGLMC G001.0423–00.0650 from Robitaille et al. (2008) are included.

2010). These nano-sized ultrasmall grains, if they are carbonaceous in nature like HAC, undergoing collisional fragmentation and full dehydrogenation, triggered by UV photons and/or shockwaves from star formation activities, could result in the creation of C_{24}. Therefore, it is not surprising that C_{24} is related to star formation activity.

Finally, we note that it would potentially be useful to compare the physical and chemical conditions (e.g., the UV starlight intensities, the hydrogen and electron number densities, and the gas temperature) of the four pointings in which C_{24} is possibly present with those of the other pointings in which C_{24} is not seen. However, it is difficult to obtain a complete census of the YSOs and their initial mass functions in these regions. Also, UV extinction prevents an accurate direct measure of the UV starlight intensities even if the UV photometric or imaging data are available (e.g., from the *Hubble Space Telescope* (*HST*)). Therefore, we prefer not to make comparisons between the environments of the four pointings and the other pointings.

4 SUMMARY

PAHs, one of the precursors of graphene, are widespread in star-forming environments. Inspired by the possible detection of C_{24} emission features at $\sim$6.6, 9.8 and 20 μm in several Galactic and extragalactic PNe, and by recent theoretical endeavors related to C_{24} in the ISM, we have searched for characteristic IR emission features of C_{24} toward the high-mass star formation region Sgr B2. We detected IR emission, with three peak wavelengths of $\sim$6.637, 9.853 and 20.050 μm toward R.A. (J2000) = 267.05855° and Decl. (J2000) = −28.01479° in Sgr B2. These three wavelengths are all very close to the most pronounced three characteristic IR emission features of C_{24}. These detected features are also accompanied by the characteristic IR emission bands of possibly C_{60}.

The three-color (21, 70 and 500 μm) images indicate that the target is probably in a warm dust environment which is heated by nearby massive stars or star clusters. The *WISE* false-color map suggests that the target source is associated with a *WISE* spot with excesses at 12 μm and 22 μm, a tracer of star-formation activity. The nearest IRAS source (IRAS 17450-2759) is 13.7″ away, and this IRAS source is an HII region candidate. The target source is also surrounded by seven YSO candidates within 5′. All these suggest that the IR emission of C_{24} could be powered by star formation activity.

Acknowledgements We thank the anonymous referee for his/her very helpful suggestions and comments which substantially improved the quality of this work. This research is supported by the National Natural Science Foundation of China (NSFC, No. 11873041) and the Hunan Provincial Innovation Foundation for Postgraduates (CX2015B213), and by the Joint Research Funds in Astronomy (U1531108, U1731106 and U1731110) under cooperative agreement between the NSFC and the Chinese Academy of Sciences and in part by the NSFC (U1731107).

References

Álvaro Galué, H., & Díaz Leines, G. 2017, Physical Review Letters, 119, 171102
Barnes, A. T., Longmore, S. N., Battersby, C., et al. 2017, MNRAS, 469, 2263
Bernard-Salas, J., Cami, J., Peeters, E., et al. 2012, ApJ, 757, 41
Berné, O., & Tielens, A. G. G. M. 2012, Proceedings of the National Academy of Science, 109, 401
Berné, O., Mulas, G., & Joblin, C. 2013, A&A, 550, L4
Berné, O., Cox, N. L. J., Mulas, G., & Joblin, C. 2017, A&A, 605, L1
Bernstein, L. S., Shroll, R. M., Lynch, D. K., et al. 2017, ApJ, 836, 229
Borowski, P. 2012, Journal of Physical Chemistry A, 116, 3866
Cami, J., Bernard-Salas, J., Peeters, E., et al. 2010, Science, 329, 1180
Campbell, E. K., Holz, M., Gerlich, D., et al. 2015, Nature, 523, 322
Campbell, E. K., Holz, M., Maier, J. P., et al. 2016, ApJ, 822, 17
Chen, X. H., Li, A., & Zhang, K. 2017, ApJ, 850, 104
Chuvilin, A., Kaiser, U., Bichoutskaia, E., et al. 2010, Nature Chemistry, 2, 450
Draine, B. T., & Lee, H. M. 1984, ApJ, 285, 89
Draine, B. T., & Li, A. 2001, ApJ, 551, 807
Foing, B. H., & Ehrenfreund, P. 1994, Nature, 369, 296
García-Hernández, D. A., Manchado, A., García-Lario, P., et al. 2010, ApJ, 724, L39
García-Hernández, D. A., Rao, N. K., & Lambert, D. L. 2011a, ApJ, 739, 37
García-Hernández, D. A., Iglesias-Groth, S., Acosta-Pulido, J. A., et al. 2011b, ApJ, 737, L30
García-Hernández, D. A., Villaver, E., García-Lario, P., et al. 2012, ApJ, 760, 107
Gaume, R. A., Claussen, M. J., de Pree, C. G., et al. 1995, ApJ, 449, 663
Ginsburg, A., Henkel, C., Ao, Y., et al. 2016, A&A, 586, A50
Ginsburg, A., Bally, J., Barnes, A., et al. 2018, ApJ, 853, 171
Grieco, V., Matteucci, F., Ryde, N., et al. 2015, MNRAS, 450, 2094
Griffin, M. J., Abergel, A., Abreu, A., et al. 2010, A&A, 518, L3
Guesten, R., & Downes, D. 1983, A&A, 117, 343

Guillois, O., Ledoux, G., & Reynaud, C. 1999, ApJ, 521, L133
Henning, T., & Salama, F. 1998, Science, 282, 2204
Henshaw, J. D., Longmore, S. N., Kruijssen, J. M. D., et al. 2016, MNRAS, 457, 2675
Higuchi, A. E., Hasegawa, T., Saigo, K., et al. 2015, ApJ, 815, 106
Houck, J. R., Roellig, T. L., van Cleve, J., et al. 2004, ApJS, 154, 18
Iglesias-Groth, S., Cataldo, F., & Manchado, A. 2011, MNRAS, 413, 213
Jäger, C., Posch, T., Mutschke, H., et al. 2011, in IAU Symposium, 280, The Molecular Universe, eds. J. Cernicharo, & R. Bachiller, 416
Kauffmann, J., Pillai, T., Zhang, Q., et al. 2017, A&A, 603, A89
Kohoutek, L. 2001, A&A, 378, 843
Kuzmin, S., & Duley, W. W. 2011, arXiv:1103.2989
Kwok, S., & Zhang, Y. 2011, Nature, 479, 80
Martin, J. M. L., El-Yazal, J., & François, J.-P. 1996, Chemical Physics Letters, 255, 7
Molinari, S., Bally, J., Noriega-Crespo, A., et al. 2011, ApJ, 735, L33
Morris, M., & Serabyn, E. 1996, ARA&A, 34, 645
Novoselov, K. S., Geim, A. K., Morozov, S. V., et al. 2004, Science, 306, 666
Pilbratt, G. L., Riedinger, J. R., Passvogel, T., et al. 2010, A&A, 518, L1
Poglitsch, A., Waelkens, C., Geis, N., et al. 2010, A&A, 518, L2
Price, S. D., Egan, M. P., Carey, S. J., et al. 2001, AJ, 121, 2819
Requena-Torres, M. A., Martín-Pintado, J., Rodríguez-Franco, A., et al. 2006, A&A, 455, 971
Robitaille, T. P., Meade, M. R., Babler, B. L., et al. 2008, AJ, 136, 2413
Rosenberg, M. J. F., Berné, O., & Boersma, C. 2014, A&A, 566, L4
Sellgren, K., Werner, M. W., Ingalls, J. G., et al. 2010, ApJ, 722, L54
Shetty, R., Beaumont, C. N., Burton, M. G., et al. 2012, MNRAS, 425, 720
Simpson, J. P. 2018, ApJ, 857, 59
Simpson, J. P., Colgan, S. W. J., Cotera, A. S., et al. 2007, ApJ, 670, 1115
Strelnikov, D., Kern, B., & Kappes, M. M. 2015, A&A, 584, A55
Tanaka, K., Nagai, M., Kamegai, K., et al. 2018, ApJS, 236, 40
Tielens, A. G. G. M. 2008, ARA&A, 46, 289
Van Kerckhoven, C., Tielens, A. G. G. M., & Waelkens, C. 2002, A&A, 384, 568
Werner, M. W., Roellig, T. L., Low, F. J., et al. 2004, ApJS, 154, 1
Wright, E. L., Eisenhardt, P. R. M., Mainzer, A. K., et al. 2010, AJ, 140, 1868
Yan, Q.-Z., Xu, Y., Walsh, A. J., et al. 2018, MNRAS, 476, 3981
Yang, X. J., Glaser, R., Li, A., et al. 2013, ApJ, 776, 110
Yusef-Zadeh, F., Hewitt, J. W., Arendt, R. G., et al. 2009, ApJ, 702, 178
Zhang, Y., & Kwok, S. 2011, ApJ, 730, 126
Zhang, Y., & Kwok, S. 2013, Earth, Planets, and Space, 65, 1069